Available online at www.sciencedirect.com
SCIENCE DIRECT®
Journal of Power Sources 117 (2003) 223–232
JOURNAL OF POWER SOURCES
www.elsevier.com/locate/jpowsour

A contact-less method to evaluate the state of charge of nickel batteries using Foucault's eddy currents

V. Mancier[a,*], A. Metrot[a], P. Willmann[b]

[a]*Laboratoire d'Electrochimie et Chimie du Solide, DTI-CNRS UMR 6107, Faculté des Sciences, B.P. 1039, F-51687 Reims Cedex 2, France*
[b]*CNES, 18 Avenue E. Belin, BPI 161, F-31401 Toulouse Cedex 4, France*

Received 23 September 2002; received in revised form 27 December 2002; accepted 30 December 2002

Abstract

A nickel hydroxide electrode and a commercial battery have been studied by a new and contact-less impedance method, based on Foucault's eddy currents, with the aim of determining their state of charge. Four different current line distributions have been employed and the impedance versus time graphs obtained show a linear variation of this impedance during charge and discharge for all configurations. This new method allows the determination of the state of charge and, furthermore some ''artifacts'' obvious on these graphs may be useful to detect a deterioration of the studied material.

Keywords: Nickel hydroxide electrode; AC impedance; Foucault's eddy currents; State of charge determination

1. Introduction

Secondary batteries are more and more widely used in consumer, military and spatial areas, at different scales from tiny elements for portable electronics to large ones for electrical vehicles. Among them, nickel hydroxide batteries, i.e. Ni/Cd and Ni/MH, are recognized for their performances and reliability.

In these batteries the output potential remains quite constant during the charge and the discharge, which can be viewed as an advantage for electronics supplies but which makes it difficult to determine their state of charge (SOC), a key problem for users. Electrochemical impedance spectroscopy (EIS) has sometimes been proposed for this determination but it appears that the spectra remain quite unchanged during most of the charge–discharge cycles, despite the changes of electronic conductivity of the nickel oxo-hydroxide electrode (NOHE) active matter (AM) [1] following the reaction:

$$NiOOH + 2H^+ + 2e^- \leftrightarrow Ni(OH)_2$$

when considering that the electronic conductivity of $Ni(OH)_2$ is known to be significantly lower than the NiOOH one. We have recently suggested an alternative method emphasizing this electronic conductivity variation, i.e. the transverse impedance spectroscopy (TIS) method, where the impedance is measured between two opposite metallic contacts soldered on the NOHE itself [2]. TIS spectra appear indeed more consistent with the SOC than the EIS ones. Nevertheless transverse impedance are usually very low, as the active matter is short circuited by the nickel substrate. This makes their measurement difficult and dependant on the quality of the soldered contacts. There is also another problem: the wires necessary to measure the transverse impedance have to cross the container, introducing practical problems for the cell tightness.

We report here results demonstrating the feasibility of an indirect evaluation of the transverse impedance, using a contact-less method based on Foucault's eddy currents. The method was firstly tested in a laboratory cell where the NOHE is spatially separated from the counter electrode and then applied on commercially available Ni/Cd batteries. A French patent has been deposited [3].

2. Principle of the Foucault's method

Foucault's eddy currents appear inside any conductor exposed to an alternative inductive field: the conductor behaves as a short-circuited secondary coil of a transformer. During such an exposition the apparent impedance (AI) of

* Corresponding author. Tel.: +33-326-913181; fax: +33-326-913195.
E-mail address: valerie.mancier@univ-reims.fr (V. Mancier).

0378-7753/03/$ – see front matter © 2003 Elsevier Science B.V. All rights reserved.
doi:10.1016/S0378-7753(03)00112-5

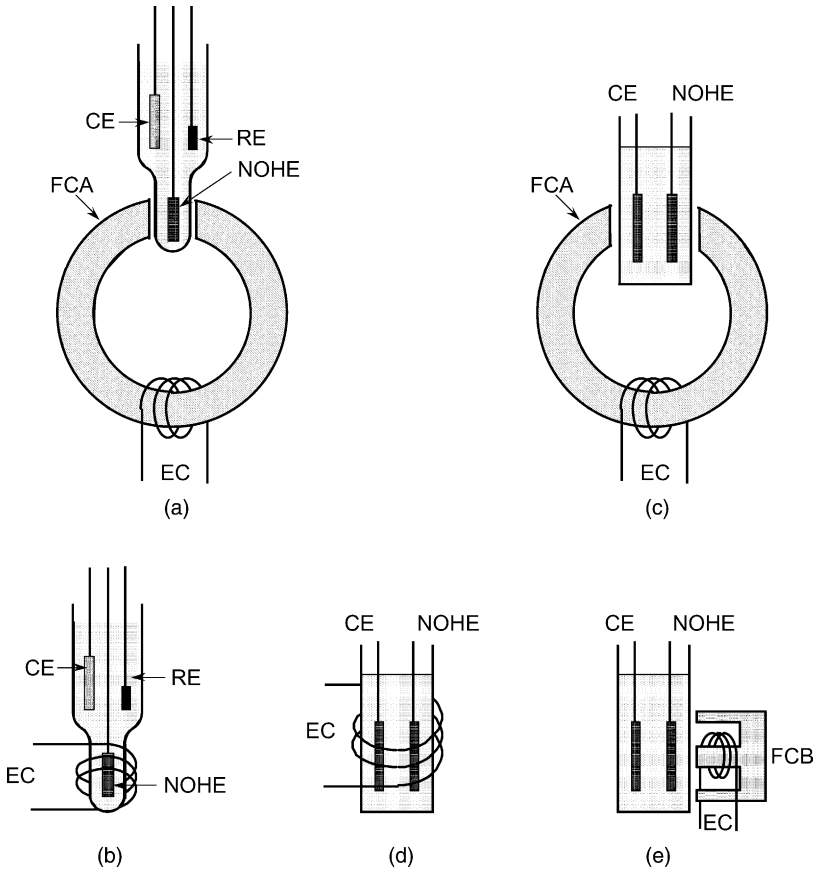

Fig. 1. Typical set-up configurations with respect to the inductive field situation vs. the electrode (perpendicular: a, c, or parallel: b, d), using (a, c, e) or not (b, d) ferrite cores, applied either to an isolated electrode (a, b) or to a complete battery (c, d, e). N.B.: the configuration e involves a mixed parallel–perpendicular field induction.

the coil emitting the field is slightly perturbed, in response to the Joule energy dissipation in the exposed material. Based on this principle, many devices may be designed to follow the conductivity changes of a planar electrode. One may consider for example the different geometrical distributions of current lines inside the electrode resulting from the position of the emitting coil with respect to the electrode, the use or not of external ferrite cores to channel the magnetic lines, etc. Five typical configurations are presented in Fig. 1, involving parallel or perpendicular field induction (the fifth one includes a mixed distribution) applied either on isolated NOHE or on commercially available batteries. Ferrite cores were used when necessary. The configuration 1a is reminiscent of a device formerly used by Zeller et al. [4] to study the conductivity of intercalated HOPG samples.

3. Experimental

3.1. Electrical set-up

The ultimate set-up includes a Wheatstone's bridge to detect the small variations of the emitting coil (EC) impedance (Fig. 2). The EC was inserted between the points 1 and 4 of the bridge and a reference coil (RC) between the points 1 and 2. An adjustable resistance (AR) was connected between the points 2 and 3 and a reference resistance (RR) between the points 3 and 4. Meanwhile the Generator G of a 1253 Solartron frequency response analyzer (FRA)

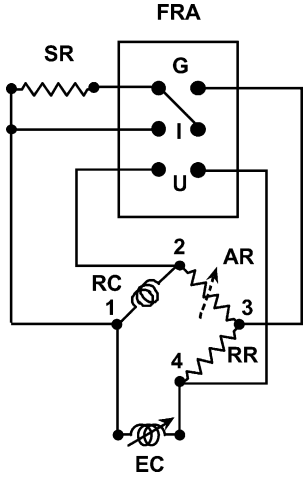

Fig. 2. Wheatstone bridge set-up used to detect eddy currents changes inside the electrode.

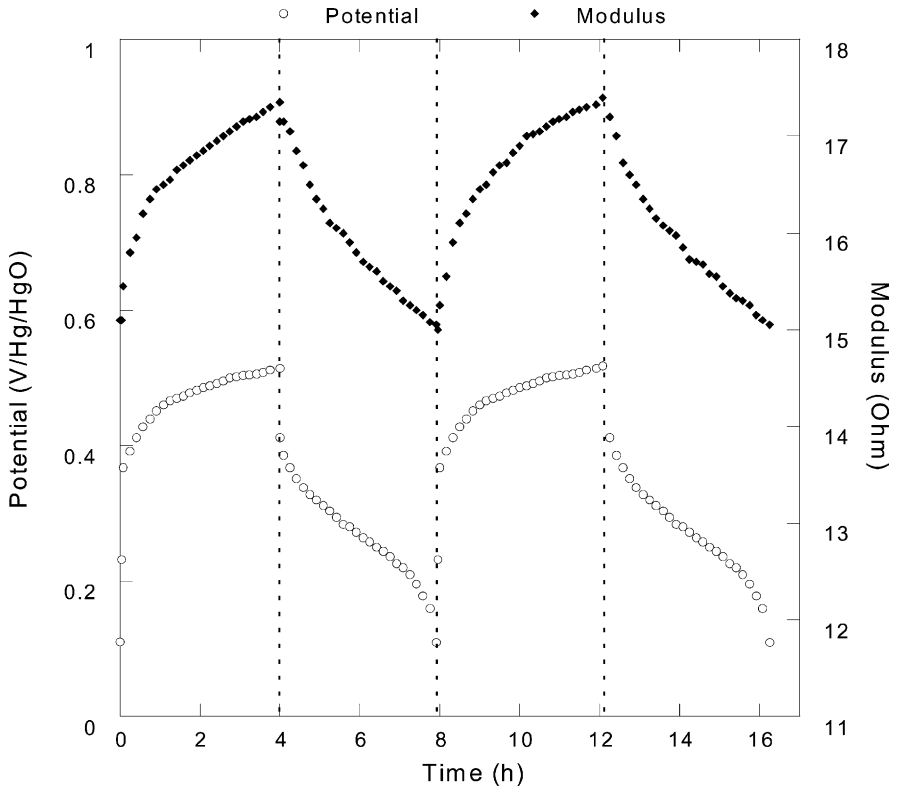

Fig. 3. Simultaneous potential and AI responses reported as functions of time during galvanostatic cycling (C/8) of an isolated felt NOHE according to Fig. 1a.

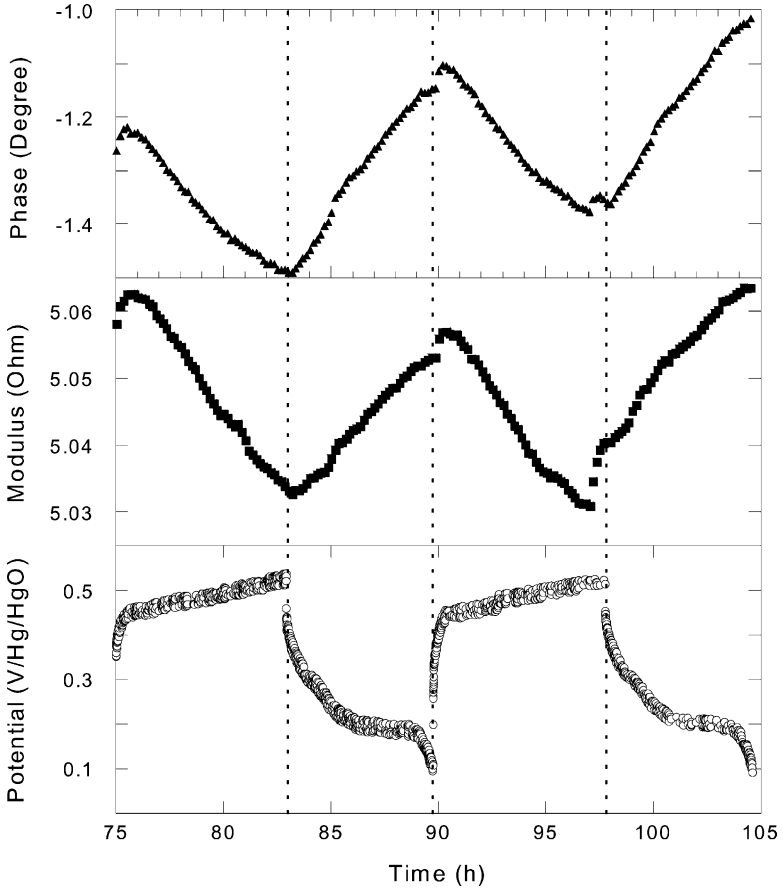

Fig. 4. Simultaneous potential and AI responses reported as functions of time during galvanostatic cycling (C/8) of an isolated felt NOHE according to Fig. 1b.

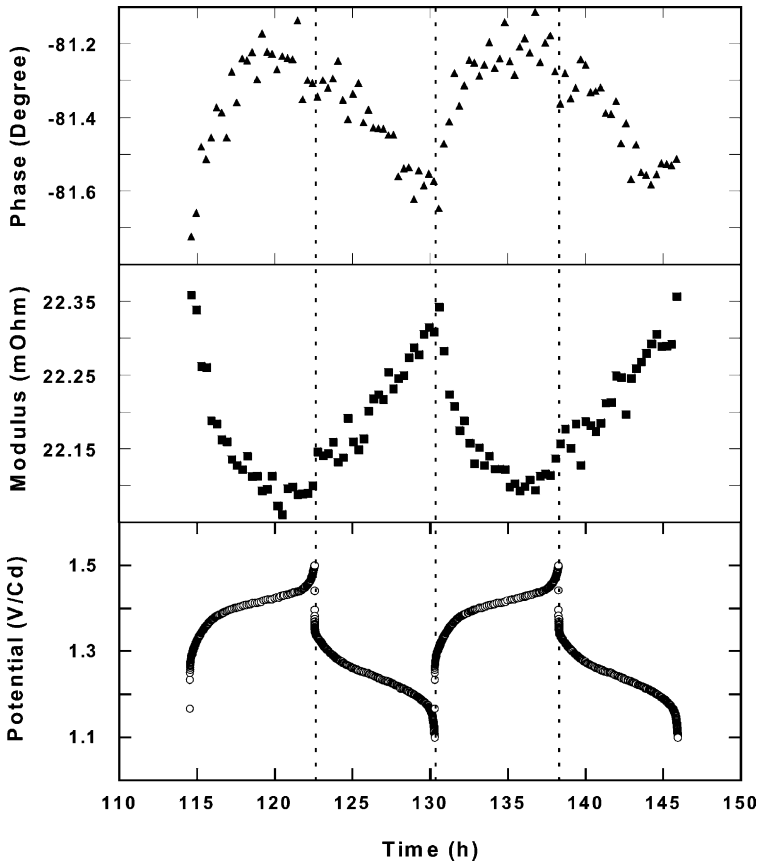

Fig. 5. Simultaneous potential and AI responses reported as functions of time during galvanostatic cycling (C/11) of a complete battery according to Fig. 1d.

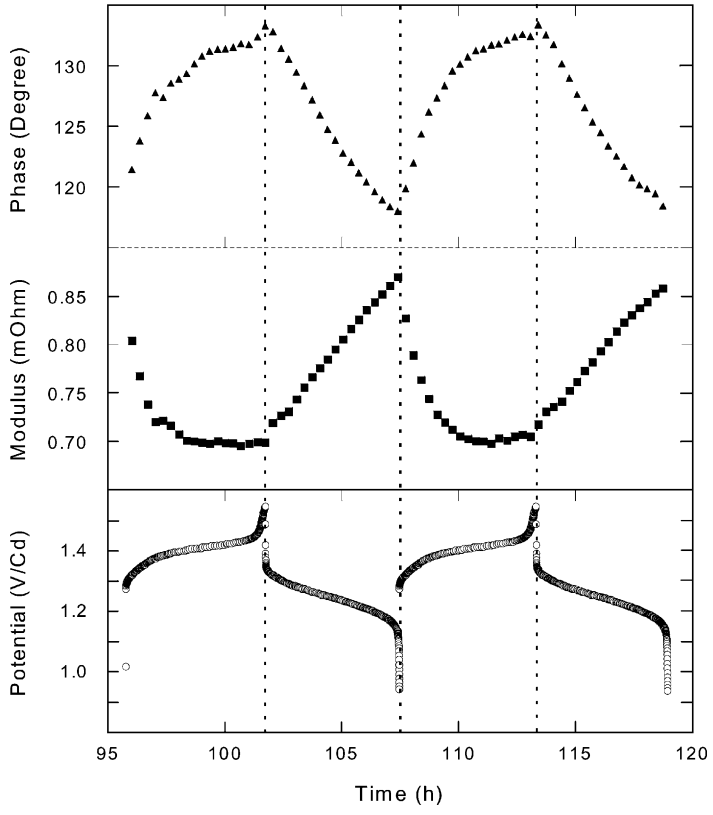

Fig. 6. Simultaneous potential and AI responses reported as functions of time during galvanostatic cycling (C/11) of a complete battery according to Fig. 1e.

was connected to the points 1 and 3, through a standard resistance (SR) used to measure the current (I) flowing in the bridge. The potential U was read between points 2 and 4. The bridge was primarily tuned, at a given frequency, in order to obtain the lowest value for (U), acting on AR. It is noteworthy that the AI computed by the FRA as U/I was only indirectly linked to the EC impedance and hereafter to the NOHE impedance, so that AI values are comparable from one experiment to another only for the same tuning conditions.

The contact-less measurements were done at fixed frequencies, during galvanostatic charge–discharge cycles,

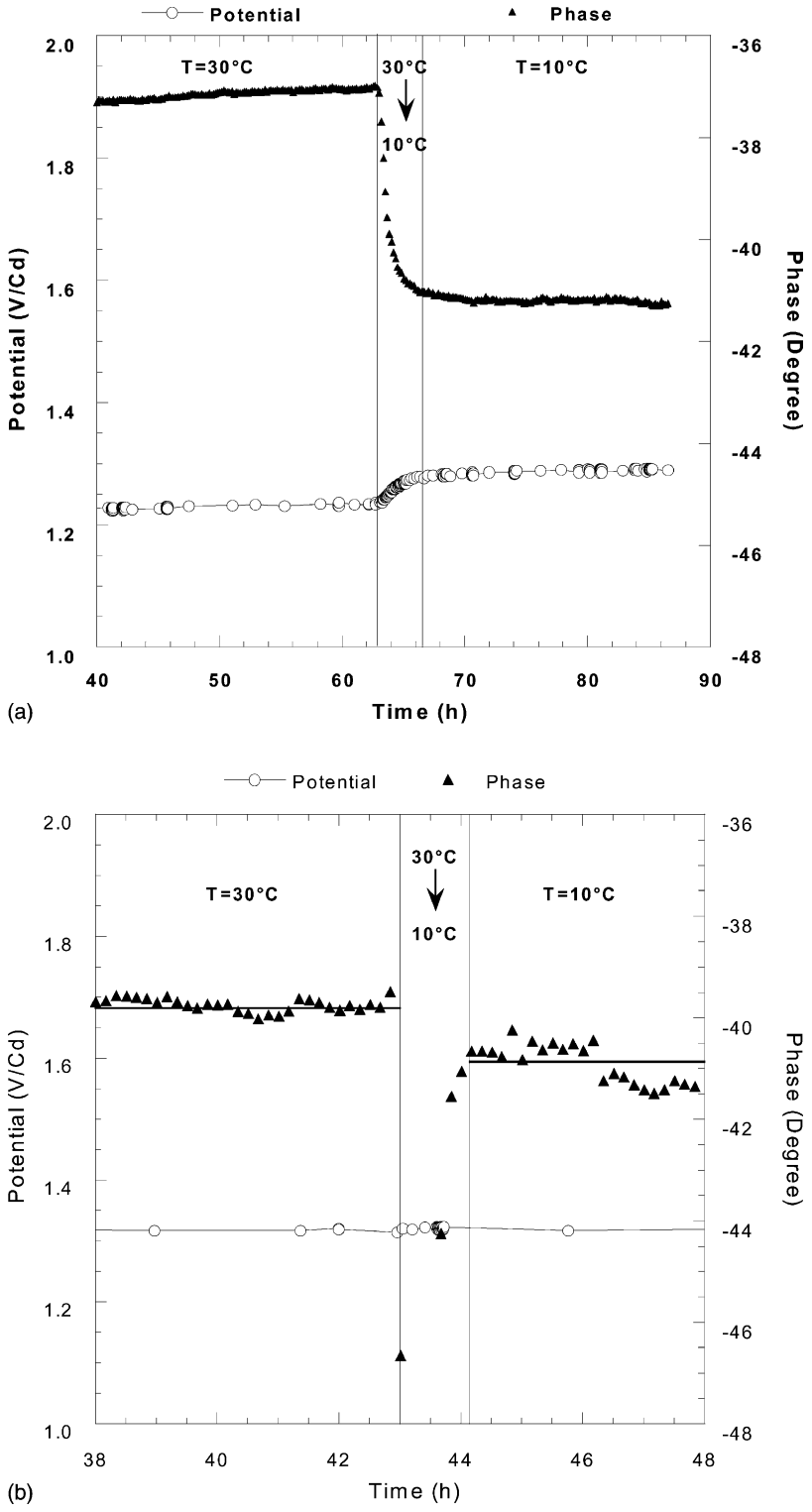

Fig. 7. Temperature influence on the AI response (phase) at zero current and two states of charge (a: 0 and b: 100%) obtained with the configuration 1e.

using a PC driven galvanostat (Mac-Pile II with a 1 A amplifier, Bio-Logic, France).

3.2. Materials

NOHE electrode (Fig. 1a and b): The studied NOHE was a commercially available felt one, manufactured by SORAPEC. Its area was 1 cm^2 and its capacity 20 mAh. The counter electrode was a cadmium electrode, with a capacity exceeding the NOHE one. The three-electrodes cell included a Hg/HgO reference electrode and a 7 mol l^{-1} KOH solution was used as electrolyte. Experiments were thermostated at 25 °C. Before its study the NOHE was submitted to formation cycles according to the manufacturer's procedure.

Nickel–cadmium cell (Fig. 1d and e): The studied battery was a SAFT VP65K one, with a nominal capacity of 6.5 Ah (charging rates were calculated using this capacity even the actual capacity was somewhat inferior due to aging effects). It included sintered nickel and cadmium electrodes, insulated from each other by a polyamide felt separator. The cell case was in polyamide. The battery was air-tight but included a valve allowing the release of gas produced during overcharge or over-discharge. Water was introduced, if necessary, through this valve to compensate its loss during overcharge, in order to maintain the KOH concentration at 5 mol l^{-1}. The cadmium electrode was here used both as counter and as reference electrode. Experiments were usually performed at 20 °C. Before the first experiment, formation cycles were done according to the manufacturer's procedure too.

Coils and ferrites: Home-made coils (generally about 100 spiral-turns) were associated with two types of ferrites cores, FCA (Fig. 1a, 20% Mn, 11% Zn, 69% Fe) or FCB (Fig. 1e, 15% Mn, 17% Zn, 68% Fe). Resulting self inductance values were: 2.11 mH (Fig. 1a), 0.247 H (Fig. 1b), 0.46 mH (Fig. 1d) and 2.11 mH (Fig. 1e).

3.3. Results

Figs. 3–6 depict result obtained near 1000 Hz with the different configurations described on Fig. 1 excepting configuration c which has not been tested. Significant results are obtained in all cases for both perpendicular and parallel inductive field configurations: the AI values (phase and modulus) vary significantly with the SOC in synchronism with current inversion times (Figs. 4–6). A different and simplified set-up was used in the case of Fig. 3, giving only the modulus of a coil-related impedance: good relationship with cycling inversion is also observed. Hence these four configurations may be used to evaluate the SOC.

Fig. 7 shows, when the EC equipped with a ferrite core FCB and the reference FCB/coil in the bridge are maintained at the same temperature, that the AI response is influenced by changes of the temperature, especially at low SOC values (Fig. 7a), but more faintly at high SOC values (Fig. 7b).

Outside these regular results some apparently odd ones have been observed, which will be discussed in the following.

4. Discussion

4.1. Theoretical assessment of the method

Qualitatively some variation of the AI with the SOC was expected but *quantitatively* a theoretical prevision appeared quite tricky, taking into account both the complex morphology of the NOHE itself and the poorly known transfer functions between its impedance and the AI response. In these electrodes the AM ($Ni(OH)_2$/NiOOH) is dispersed on sintered or fibrous nickel substrates which act as electron collector, with a conductivity largely superior to the AM one. So one might fear that most of eddy currents would flow inside the substrate, avoiding the active matter and so remaining independent of the SOC.

The results presented, in agreement with previous TIS ones [2], demonstrate that this is not the case. This fortunate

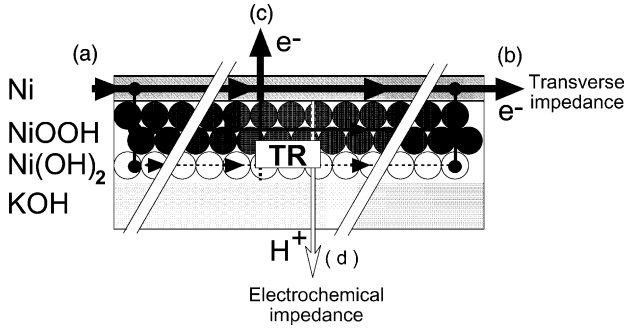

Fig. 8. Scheme of the conductivity paths inside NOHE involved during transverse (a, b) and electrochemical (c, d) impedance measurements.

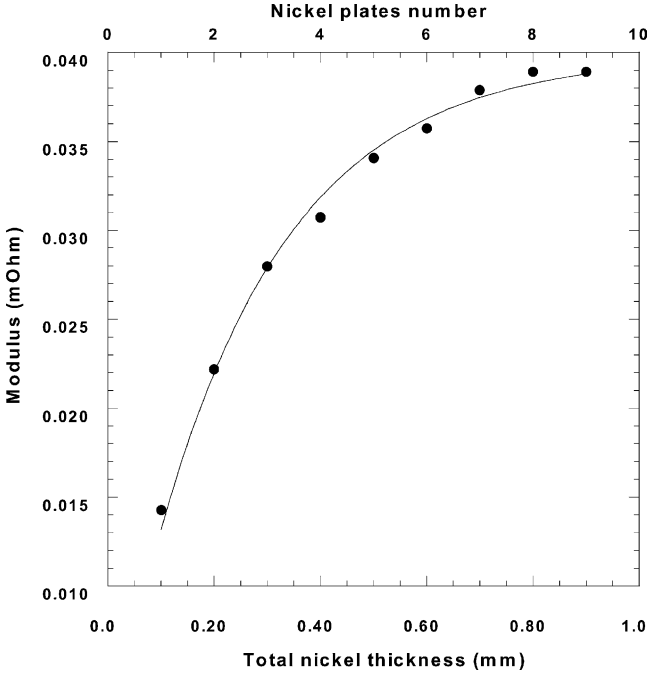

Fig. 9. AI response (modulus) vs. the nickel plates total thickness obtained with the configuration 1e.

fact may result from the balance of substrate and AM resistances ensuring the optimization of energy/mass and power/mass ratios in manufactured electrodes. Another gratifying observation is the quasi-linear variation of AI with the SOC during most of the discharge, which is in agreement with TIS measurements.

The reasons of the enhanced sensitivity of the TIS method towards the SOC, with respect of the EIS one, have been thoroughly discussed in a previous paper [2]. In a simplified view one considers the double electronic/protonic conductivities of the AM. The differences between EIS and TIS (at least during two-phases transformations, the most significant part of the SOC to be practically gauged) are illustrated in Fig. 8. Any *electrochemical* current involves *serial* electronic and protonic currents interacting through a "transfer resistance" localized at the frontier between the charged and discharged matters. On the contrary *transverse* currents flow simultaneously in the charged and discharged matters, mainly through *parallel* electronic paths. Assuming now that the electronic conductivity of NiOOH is plainly larger that of $Ni(OH)_2$, but only slightly superior to the protonic conductivity, and that electrochemical currents choose the less resistive paths, one may explain why the NiOOH phase remains on the nickel side, which acts as an electron sink. Furthermore, one can explain that electrochemical impedance are less contrasted than transverse impedance, as electrochemical currents avoid the electronically highly resistive $Ni(OH)_2$ phase. Hereafter quasi-linear variations of transverse eddy currents versus the SOC, during two-phases transformations, are also easily understood.

Another question arises, related to skin effects: did eddy currents penetrate sufficiently the NOHE at the frequencies used in order to allow meaningful measurements? Indeed a theoretical calculation of the skin depth δ of the NOHE is difficult, due both to the complex active matter distribution (a few micrometers thick on the felt or sintered nickel substrate), and to the ferromagnetic nature of the metal. Moreover the lack of precise data on AM (especially

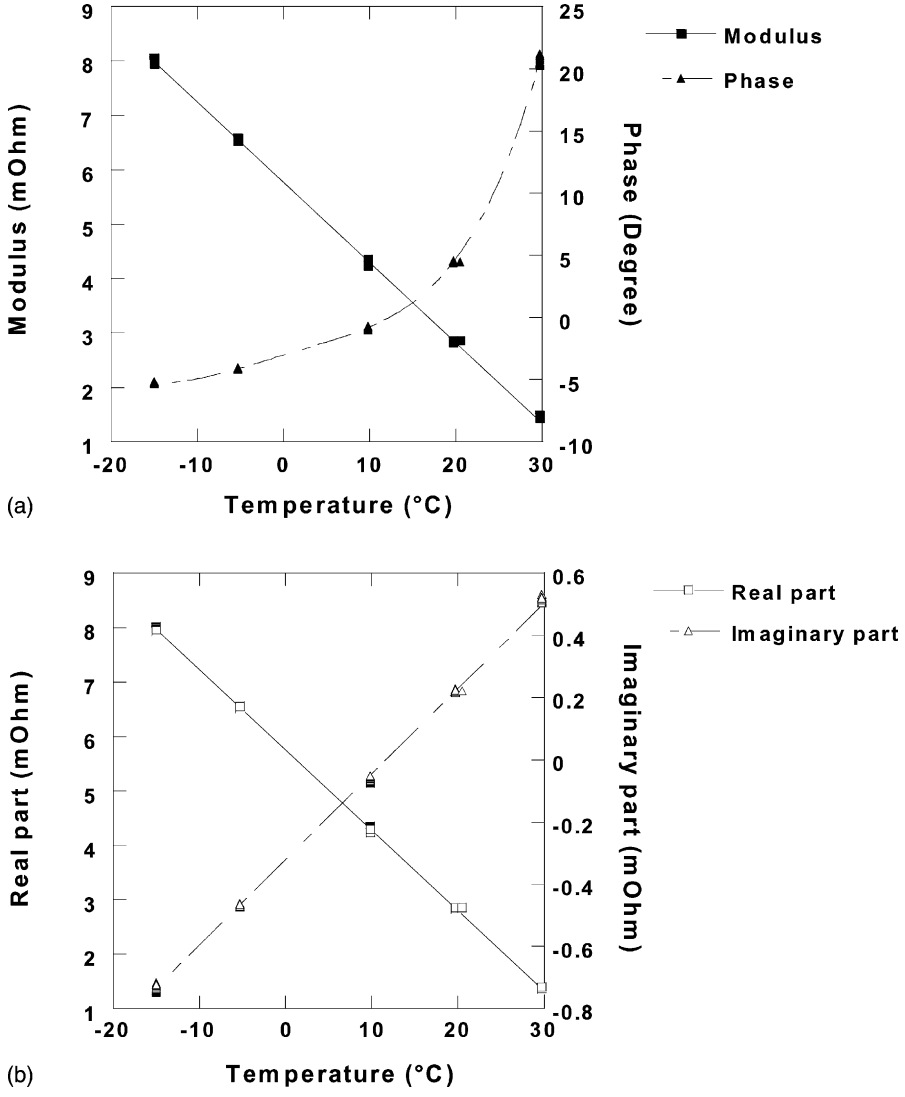

Fig. 10. Temperature dependence on the AI responses of a coil used in configuration 1e.

NiOOH) resistivity and magnetic properties makes accurate calculations rather difficult.

Some experimental measurements have been done previously, piling up 0.1 mm thick nickel plates in front of the EC, at 1000 Hz (configuration of Fig. 1e). The curves of AI versus the plates total thickness e (Fig. 9) could be fitted according to the exponential law:

$$\mathrm{AI} = \mathrm{AI}_\infty \times \left(1 - \exp\left(-\frac{e}{\delta}\right)\right)$$

where AI_∞ is the limit value of AI in the case of infinite metal thickness, taking:

$\delta = 0.25\,\mathrm{mm}$

This value appears as a lower limit, considering the porous texture of the nickel substrate and the higher resistivity of the active matter.

Referring now to the theoretical formula:

$$\delta = \left(\frac{\rho}{\pi\mu f}\right)^{0.5}$$

i.e. numerically if expressing δ in mm (in S.I. units), ρ in μΩ cm and taking into account the relative permeability:

$$\mu_\mathrm{r} = \frac{\mu}{\mu_0}, \quad \text{where } \mu_0 = 4\pi 10^{-7}\,\mathrm{N\,A^{-2}}$$

$$\delta(\mathrm{mm}) = 50.3\left(\frac{\rho}{\mu_\mathrm{r} f}\right)^{0.5}$$

Taking $\rho(\mathrm{Ni}) = 6.9\,\mathrm{m\Omega\,cm}$ [5] and μ_r (Ni) = 110 (initial relative permeability [6], this permeability depending on the magnetic field), one obtains at 1000 Hz:

$\delta = 0.40\,\mathrm{mm}$

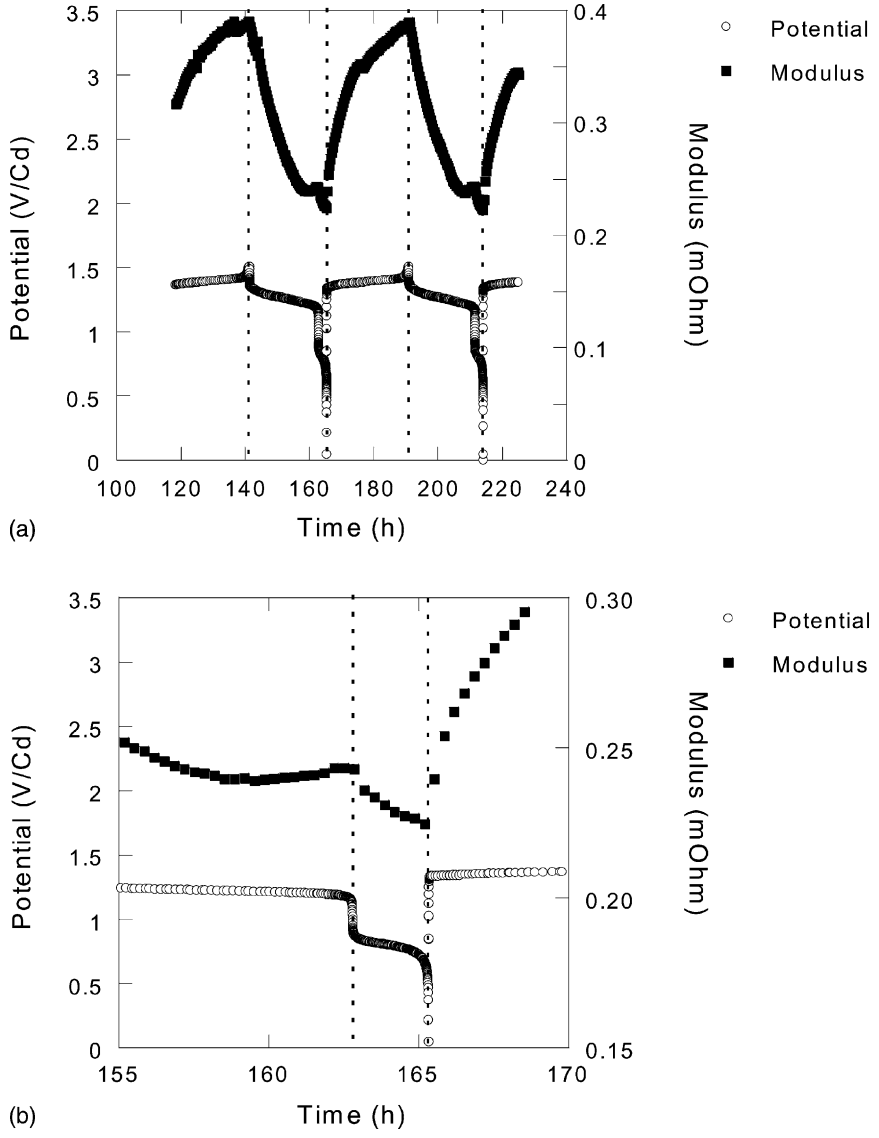

Fig. 11. Discrepancies of the AI (modulus)–SOC relation correlated to a second plateau on C/32 current cycling obtained with the configuration 1e. The Fig. 11b is a zoom of the end of the discharge.

in relative agreement with the previous one. Consequently one may consider that eddy currents penetrate the whole electrode, the thickness of which is about 1 mm. This is of course only a rough estimate as only nickel has been considered.

Another problem may then concern the variation of the ferrite cores permeability with the temperature. Fig. 10 shows for example the temperature dependence, in the absence of any cell, of the AI of an EC equipped with a ferrite (FCB) core when the reference ferrite/coil in the bridge was maintained at the constant temperature of 20 °C. Practically, these variations can be minimized using a differential set-up with two coils held at the same temperature (as in the case of Fig. 7) and corrections may be made through a software program. Similarly the AI intensity dependence is not clearly understood: it may be due to non-equilibrium states.

4.2. Odd behavior and artifacts

Divergences from the regular AI–SOC relation seem to be related either to discrepancies of the charge–discharge processes, i.e. overcharge or second plateau appearance, or to artifacts due to mechanical deformations of the cell.

The so called second plateau phenomenon appears on aged cells especially when they have been overcharged [7–10]. Discrepancies of the AI–SOC relation and of the charge–discharge curve are observable on the Fig. 11. A zoom shows that the second plateau apparition is preceded by a slight augmentation of the AI modulus. In other words, a slight inversion of the AI modulus variation during discharge prognosticates a deterioration of the cell, which is associated with the second plateau apparition. In fact this phenomenon, which appeared firstly as troublesome, may be used to watch over the cell health.

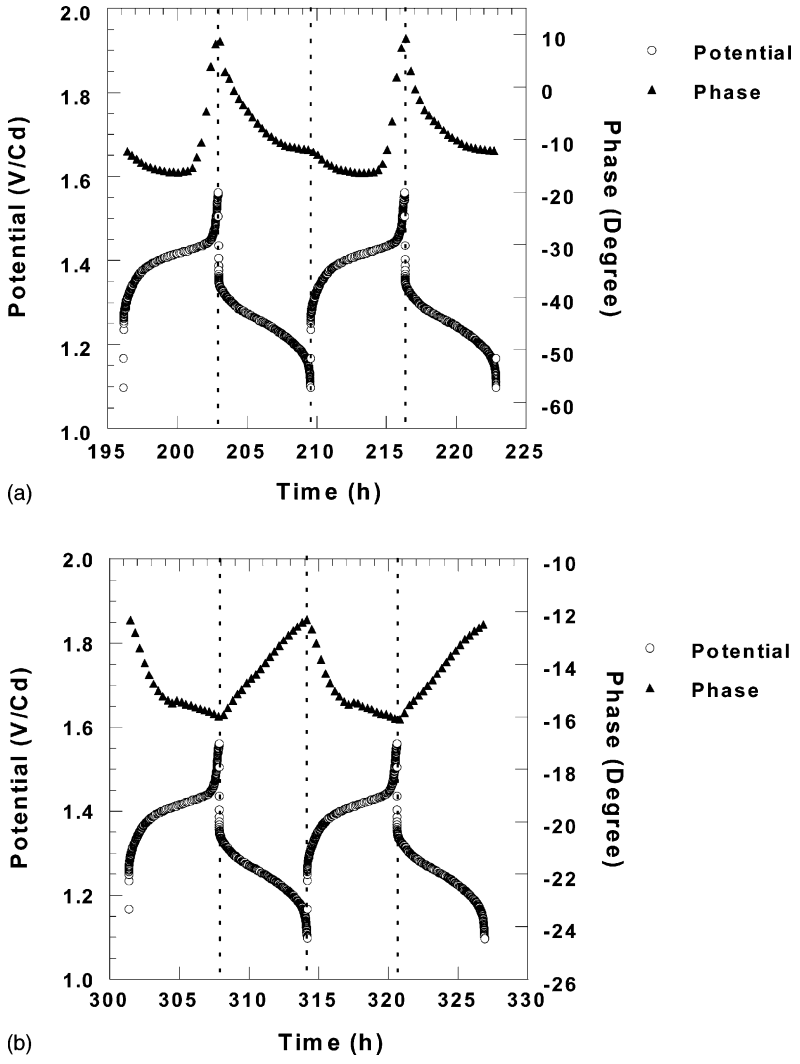

Fig. 12. (a) Discrepancy of the AI (phase)–SOC relation observed in case of a mechanical deformation of the cell over pressure with closure of the safety valve; (b) normal response of the signal. These two graphics are obtained with the configuration 1e.

Artifacts due to mechanical deformations of the cell were also observed during or after over-charge or over-discharge of the SAFT VP65K cell, using an external ferrite core (Fig. 1e): due to gas evolution (O_2 or H_2) the polyamide case was slightly expanded and therefore the ferrite core was moved away from the NOHE, modifying the AI response. This interpretation was confirmed by the disappearance of the phenomenon when the safety valve was opened (Fig. 12).

5. Conclusion

The relevance of a new contact-less method to evaluate the state of charge of nickel secondary batteries, i.e. Ni/Cd and Ni/MH ones, has been demonstrated. Indeed, the method can be applied to other cells, provided a sufficient difference exists between the electronic conductivities of the charged and discharged states of an electrode. From a fundamental point of view the method has been assessed on the basis of a previous analysis of the transverse impedance of the nickel oxo-hydroxide electrode, i.e. its impedance between two opposite soldered electrical contacts [2]. The presented experimental set-up may undoubtedly be improved, miniaturized or simplified for particular applications.

References

[1] V. Mancier, A. Metrot, P. Willmann, Electrochim. Acta 41 (1996) 1259.
[2] V. Mancier, A. Metrot, P. Willmann, Electrochim. Acta 47 (2002) 1633.
[3] P. Willmann, A. Metrot, V. Mancier, French Patent No. 2,737,923 (1997).
[4] C. Zeller, A. Denenstein, G.M.T. Foley, Rev. Sci. Instrum. 505 (1979) 602.
[5] D.R. LIDE, CRC Handbook of Chemistry and Physics, 75th ed., CRC Press, 1995.
[6] W.F. Brown, Magnetic materials, handbook of chemistry and physics, in: Condon, Odishaw (Eds.), McGraw-Hill, Chapter 8, 1958.
[7] R. Barnard, G.T. Crickmore, J.A. Lee, F.L. Tye, J. Appl. Electrochem. 10 (1980) 61.
[8] N. Sac-Epee, Doctorate Thesis, University of Picardie, France, 1997.
[9] V. Mancier, P. Willmann, A. Metrot, J. Power Sources 85 (2000) 181.
[10] C. Leger, C. Tessier, M. Menetrier, C. Denage, C. Delmas, J. Electrochem. Soc. 146 (1999) 924.